Adaptive null test system using a ferrofluid deformable mirror

Daniel B. Landry, Denis Brousseau, Simon Thibault*, Ermanno F. Borra
Center for Optics, Photonics and Laser (COPL), Département de Physique, de Génie Physique et d'Optique, Université Laval, Québec, QC G1V 0A6, Canada

ABSTRACT

With the growing number of complex-shaped lenses, aspheric and freeform surfaces, the demand for an appropriate and cost effective measurement technique to test these high quality components is still very high. Ferrofluid deformable mirrors (FDMs) offer a promising alternative. However, high accuracy profiles produced by FDMs have only been demonstrated in a closed-loop system which is inappropriate for metrology applications as it requires an additional measurement instrument and complicates the setup. Consequently, a FDM open-loop driving technique which maintains good precision while being simple, robust and stable, is required. In the following paper, we present a new active null test system based on a FDM for the testing of deep aspheric surfaces. We show a new driving method which provides an accurate open-loop operation mode of a FDM. We demonstrate that the method gives a significant improvement in comparison with the normalized influence function method. The results are promising enough to consider an active null test configuration for measuring optical components having high sag departures or complicated continuous profiles.

Keywords: Metrology, asphere, deformable mirrors

1. INTRODUCTION

Aspheres have become a common element of complicated optical systems. Even though techniques for their fabrication allow very good accuracy [1], testing such optics is still an issue and their design still requires a lot of careful thinking. Computer generated holograms (CGHs) are commonly used for aspheric lens null testing. However, these optical components suffer from limitations [2], especially with strong aspheres. Null testing of these aspheres requires the production of wavefronts having several wavelengths of departure. This often requires expensive and complicated setups or components.

However, a proof of concept was made using deformable mirrors in lens testing [3], but again, these systems are limited in sag departure and therefore do not offer good enough improvement to compete with CGHs. In parallel to this, a new type of deformable mirrors able to produce wavefronts having several wavelengths of amplitude and low residual error has been developed [4]. Experiments have shown that these so-called ferrofluid deformable mirrors (FDM) can be considered as suitable candidates to compete with CGHs in areas where they are difficult or impossible to use.

There is still an important issue to overcome before using FDMs for null testing. The current driving method of FMDs uses regular influence matrix control as shown in [5], but does not guarantee open-loop accuracy. A serious improvement of open-loop driving is required to consider FDMs for optical testing.

In the following sections, we present a new driving method of FDMs that promises to be an improvement in using these deformables mirrors for null tests. Section 2 will present the test configuration and explains the accuracy requirements. Section 3 describes the major sources of errors of the regular influence matrix control which lead to the new driving technique. Section 4 shows some preliminary results using the new driving technique. We conclude that FDMs used in conjunction with this new control technique is promising in the case of steep aspheres testing.

2. MOTIVATION FOR CONTROL IMPROVEMENT

As mentioned before, precision testing of aspheres is usually done using CGHs which do not offer any kind of adaptability. The design of a CGH is made for given conditions (e.g. shape and wavelength) that cannot be changed afterwards. As a matter of fact, CGHs are strongly wavelength sensitive and designed for only one FOV. With costs

around 15K$ a piece, producing several CGHs to cover a broad range of wavelengths and/or FOV can become cost prohibitive. This problem can be overcome using a single adaptive component.

Null test setups are based on a simple idea; an input light beam can be characterised by a known wavefront (usually a plane-wave) refracted or reflected on at least a test component and a nulling component. If the tested component possesses the exact theoretical targeted shape, the wavefront coming out of the system is exactly the same as the one which entered, as the nulling component nulls the effect of the tested optics. Therefore, any departure of the output wavefront in comparison with the input directly shows the defects on the tested component.

However, the resulting accuracy must be equal or better than the accuracy of the nulling component. For the opposite scenario, it would be impossible to tell if the error originated from the nulling or the tested component. Typically, FDMs driven by a standard influence matrix method generate surfaces with accuracies of about one wavelength (at 632.8 nm). To be a good candidate, a FDM needs to be able to produce surfaces with accuracies between $\lambda/5$ and $\lambda/10$. Of course, one can target applications that include steep deformations even though the accuracy of the surface is not optimal. But as the accuracy gets better, the range of applications increases rapidly.

3. DEFINING A NEW DRIVING TECHNIQUE

3.1 Standard driving technique

A wavefront $\mathbf{w}_m$ produced by the FDM is given by a linear combination of the individual response functions of the actuators in the matrix form:

$$\mathbf{w}_m = \mathbf{H}\mathbf{a} \tag{1}$$

where **H** is the influence matrix and **a** is a vector made of the control signals (currents) of the actuators. Each column of the control matrix **H** represents the response function of a single actuator shifted to its corresponding location on the hexagonal grid, while each row of **H** corresponds to a single wavefront data sample. The matrix **H** is usually rectangular and needs to have more rows (data samples) than columns (actuators). For a given targeted wavefront **w**, the solution for minimum variance of Eq. (1) gives the following current vector to supply to the FDM:

$$\mathbf{a} = \left(\mathbf{H}^{\mathbf{t}}\mathbf{H}\right)^{-1}\mathbf{H}^{\mathbf{t}}\mathbf{w} \tag{2}$$

where the superscript **t** denotes the transpose matrix operation.

3.2 Error sources

In order to improve the precision, influence functions were studied in detail. For example, the measured amplitude of each pixel of the influence functions was analysed when the input voltage (actuator command) was varied from -10V to +10V. This analysis was done with different command conditions on the neighbouring actuators. These measurements helped to find two major non-linearity issues known as the scaling and coupling errors.

3.2.1 Scaling error

A scaling error implies that the system is not perfectly linear in response and therefore, some higher order polynomial terms must be taken into account when a better and more accurate surface is needed. Hence, a polynomial fit has been performed on every single pixel of the wavefront measured for input voltages of -10V to 10V. It was found that the fitting coefficient improved with second and third order fit. Fourth order terms and higher were not giving any significant improvement in accuracy. With a third order fit, the R^2 was always fairly close to unity. We can see in Fig.1a that a linear fit is not optimal and that the error can get as high as 0.05 μm on a single actuator. With contribution from all 91 actuators, the total error can be easily ten times bigger over the full pupil diameter. The fit does not represent the true method used to predict the shape of the influence function, which normally presumes a linear regression passing through the origin and a measured point. Figure 1 b shows a linear regression passing by (0,0) and the point measured at 1V and we see that errors get even bigger at large scaling, up to more than 0.1 μm per actuator. However, in Figure 1c

we note that a third order fit is much better. Nevertheless, compute the inverse matrix of such an equation is not easy. Thus, only considering higher orders would not be appropriate for easy calculation of a set of voltages.

a)

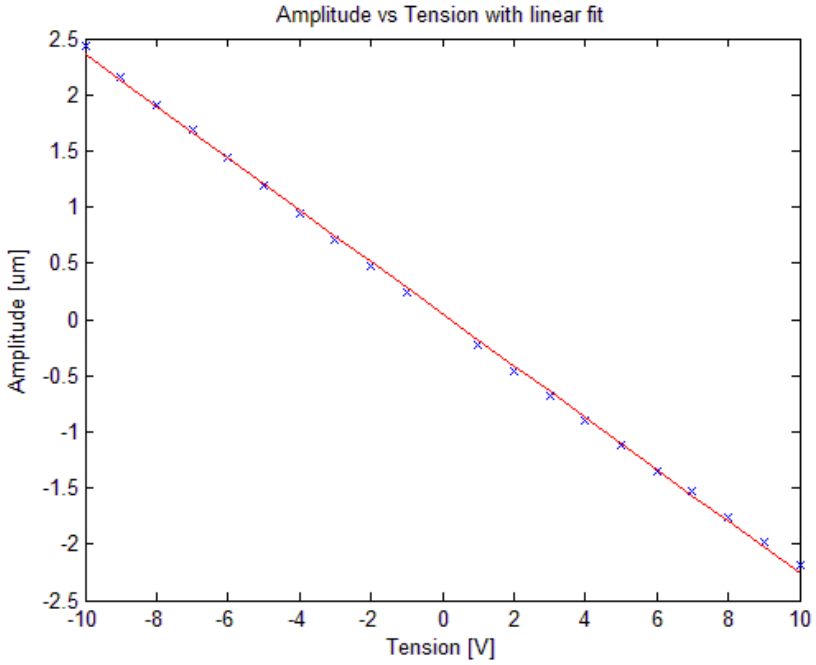

b)

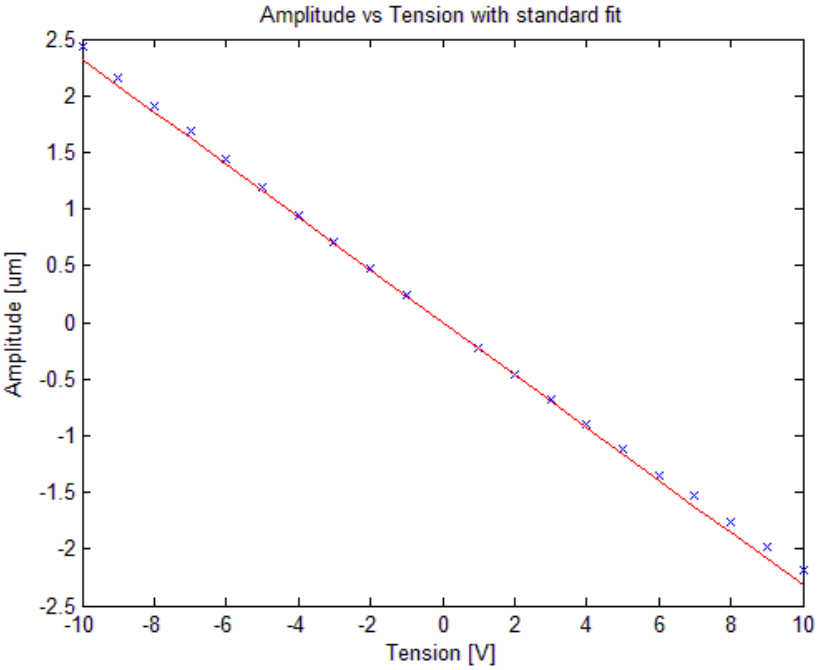

c)

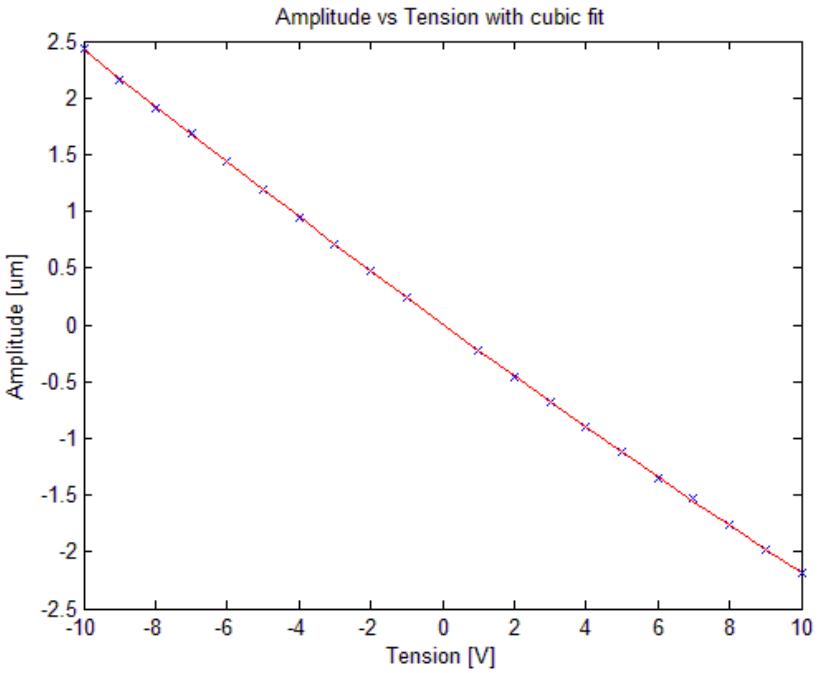

Figure 1: a) Linear fit for one pixel of the wavefront measured with voltages ranging from -10V to +10V. R^2=0.9993 by equation y=-0.2309x+0.05034. b) Linear fit of the same data. R^2=0.9981 by the equation y=-0.2319x. c) Cubic fit of the same data. R^2=1 by the equation y= 1.463e-005x^3+0.001136x^2-0.2319x+ 0.006585.

3.2.2 The coupling error

Another non-linear issue that reduces the accuracy can be noticed when analysing the relation between voltage and amplitude of the wavefront pixels when the closest neighbours have different input conditions. This slight change produces errors of comparable amplitude than that of the scaling error. This can generate errors of a few wavelengths when summed over all the 91 actuators.

It is very complicated to overcome the coupling problem because good knowledge of the coupling condition is needed. Also, in most cases, it is very difficult to derive a general mathematical equation which takes coupling into account. The coupling error has not been part of our study yet but certainly needs investigation. Also, the methods used are all based on an empirical approach and deriving an appropriate relation would probably require some theoretical investigation.

3.3 RIM technique

The principle of the RIM technique is to use the fact that the actuator response is fairly linear, even when the coupling and scaling error are taken into account. Whichever condition of a measurement, one can approximate the relation between amplitude and input voltage from another one taken close to it. For example, if we measure the influence function at 8 and 9V, the linear relation between these two measurements gives a fairly good approximation of the relationship between amplitude and voltage for this particular voltage range. Therefore, one needs to build a lookup table containing several measurements made at different conditions of coupling and input voltage. The new slope vector can replace the influence function of a given actuator in the influence matrix and be used to accurately calculate the current.

It seems though that there is still some information missing. We don't know these conditions before any calculation and we need these conditions for any calculation. This problem can be overcome using the standard technique. It is well known that the standard technique does not predict the required input voltages with very good accuracy, but it still provides a valid approximation, good enough to find where to look inside the lookup table. We also have to deal with a more complicated linear relation since we now have the relation y=ax+b instead of y=ax. Going through the calculation steps shows that we can derive an algorithm that can deal easily with this.

For any linear segment between two measurements, the slope of the wavefront amplitude versus voltage input will always be

$$\frac{\mathbf{W}_f - \mathbf{W}_i}{\mathbf{V}_f - \mathbf{V}_i}, \tag{3}$$

where *i* and *f* stand for initial and final. However, the y-intercept will not necessarily be 0 because the linear relation needs to pass exactly through our measured points (wavefronts).

From the general linear fu**n**ction

$$A = mx + b\,, \tag{4}$$

we can write

$$\mathbf{W}_i = \frac{\mathbf{W}_f - \mathbf{W}_i}{\mathbf{V}_f - \mathbf{V}_i}\mathbf{x}_i + \mathbf{B}. \tag{5}$$

We easily find that

$$\mathbf{B} = \frac{\mathbf{W}_f\mathbf{V}_i - \mathbf{W}_i\mathbf{V}_f}{\mathbf{V}_f - \mathbf{V}_i}, \tag{6}$$

Obviously, **B** and **A** are matrices having identical dimensions.
Matrix wise, the calculation is less straightforward; the individual elements of **B** need to be computed separately:

Table 1: Graphical representation of the wavefront vector with calculation at every pixel.

$$\begin{bmatrix} A_{11} * V_1 + B_{11} + A_{12} * V_2 + B_{12} + \ldots \\ A_{21} * V_1 + B_{21} + A_{22} * V_2 + B_{22} + \ldots \\ A_{31} * V_1 + B_{31} + A_{32} * V_2 + B_{32} + \ldots \\ \ldots \end{bmatrix}$$

However, one can calculate it this way:

$$\mathbf{W} = \mathbf{A} * \mathbf{V} + \mathbf{B} * \mathbf{1}, \tag{7}$$

where **1** (vector of all ones) is a column matrix having the same number of lines as the number of columns of **B**, containing only 1 entries, so **B*1** exists.

Now, **V** is given by:

$$\mathbf{V} = \mathbf{H}^{-1} * \left(\mathbf{W} - \mathbf{B} * \mathbf{1}\right), \tag{8}$$

where $\mathbf{H}^{-1}$ is the pseudo inverse of **H** and needs to have more rows than columns.

4. PRELIMINARY RESULTS

The procedure was tested in a very simple situation to verify the viability of the approach. To do so, a target shape was needed. Instead of targeting a random wavefront, one can measure one generated with a random set of input voltage and then ensure that the targeted shape can be perfectly generated by the mirror. Also, as a preliminary test, it was decided to minimise non linear effects like coupling. Only two actuators were used with low voltages at two different cases.

Case 1: [2.65V, -1.85V]
Case 2: [-3.25V, 0.65V]

The main idea was to compare different techniques of voltage calculation and compare the calculated values to the input voltages used for the each specific case. The results can be seen in Figures 2 and 3.

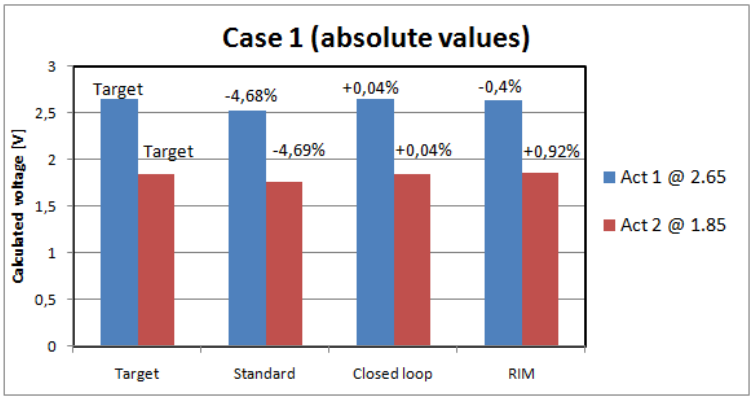

Figure 2: Comparison of the different input voltage measured using three different techniques; standard calculation, closed-loop and RIM for case 1 defined in text.

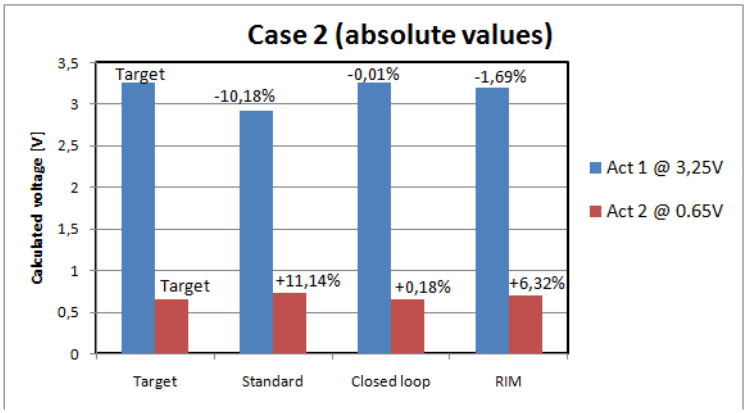

Figure 3: Comparison of the different input voltage measured using three different techniques; standard calculation, closed-loop and RIM for case 2 defined in text.

The three techniques for input voltage calculation were compared and, as expected, closed loop remains the most accurate, followed by RIM and finally standard technique. In case 1, difference between calculated and theoretical values has about the same relative error for both voltage values for a given technique. Error for closed-loop is lower than 0.5%, less than 0.1% for RIM and about 5% for the standard technique. In this case, we see a very good amelioration of accuracy with RIM. For case 2, errors aren't exactly the same for both voltages. Standard techniques generates an error higher than 10% while closed-loop is lower than 0.2% and RIM is about 2% and 6% depending on the voltage. This

difference can be explained by the fact that one of the voltage was of low value. Indeed, all measurements contain noise which can contribute to significant errors in calculation of low input voltages.

However, it is clear that the RIM technique seems to greatly improve accuracy on input voltage calculation. A deeper investigation would definitely be required, using all actuators in several different coupling and input voltage conditions. Absolute error on the full wavefront would also be a better measurement for comparison. This is part of the actual work being done to complete the research in this area.

5. CONCLUSION

In this paper we introduced a new driving technique which seems to improve the accuracy on input voltage calculation needed to generate a specific target shape on a ferrofluid deformable mirror. Motivation for such an improvement was explained as were the two major non-linear effects, the coupling and scaling errors, affecting accuracy. The RIM technique was described and results from a simple preliminary experiment showed that the technique seems to be performing well on improving calculation accuracy. Tests using all actuators in several coupling and voltage conditions are scheduled.

REFERENCES

[1] Schindler, A., "Precision optical asphere fabrication by plasma jet chemical etching (PJCE) and ion beam figuring", Proc. SPIE 4451, 242-248 (2001).
[2] Arnold, S.M. "Figure metrology of deep general aspherics using a conventional interferometer with CGH null", Proc. SPIE 2536, 106-116 (1995).
[3] Curatu, E.O., "Tolerancing and testing of CGH aspheric nulls", Proc. SPIE 3782, 591-600 (1999).
[4] Brousseau, D., Borra, E. F., Rochette, M. and Landry, D. B. "Linearization of the response of a 91-actuator magnetic liquid deformable mirror", Optics Express, vol. 18, n^{o}. 8, 8239-8250 (2010).
[5] Moore, K. E. and Lawrence, G. N., "Zonal model of an adaptive mirror", Applied Optics, vol. 29, n^{o}. 31, 4622-4628 (1990).

*Corresponding author: simon.thibault@phy.ulaval.ca